System Identification of Human Dynamics Using Periodic Impedance Models During Physical Interaction

Khandaker Nusaiba Hafiz, 1 Terence Sanger2 and Jonathan Realmuto1

Abstract—Human impedance models have emerged as a powerful framework for describing behavior based on the kinematic (generalized displacement/velocity) and kinetic (generalized force/torque) relationship, and such models have become essential for the rehabilitation sciences, and the development of advanced prosthetic and orthotic devices. However, given that most techniques include a perturbation-based protocol for system identification, a major challenge is extending the impedance modeling framework to more natural and realistic settings. In this paper, we introduce an impedance model with periodic terms for the stiffness and virtual trajectories. This allows us to fit the model without perturbations during periodic tasks. Using a single-degree-of-freedom forearm rotational haptic manipulandum, we fit our model to N=10 participants during dynamic physical interaction in four different virtual environments. Our model provides an excellent fit (average $R^2 = 0.99$) to the underlying data with minimum parameter variation across participants suggesting the periodic impedance model can accurately capture human dynamic behavior.

I. INTRODUCTION

The human neuromusculoskeletal system is capable of generating intricate, efficient movements while physically interacting with the environment [1]. These physical interactions are facilitated by direct modulation of our joint impedances (e.g., stiffness and dampening characteristics) in response to changing environmental requirements [2]. Impedance also plays a central role in maintaining postural and movement stability [3], and in learning new tasks [4]. System identification of human joint impedance, including during walking, running, reaching, and grasping can help elucidate how and why humans modulate impedance, provide a better understanding of the mechanisms of motor control and coordination, help to identify impairments in neuromuscular function, and lead to new rehabilitation strategies.

The standard approach to human joint impedance estimation is the mechanical perturbation method [5]–[7]. In this method, controlled mechanical disturbances are applied to a joint, and the joint's response to these perturbations is analyzed to gain insights into its stiffness, damping, and inertial properties. This method is not well suited for general system identification in various motions, and is impractical for real-time impedance estimation. Humans modulate limb stiffness when interacting with diverse objects [8] and

This research was funded by NSF award CMMI 2221315.

this adaptability suggests impedance modulation allows for customization according to specific task demands, achievable through adjustments in mechanical attributes, including muscle activation levels or alterations in joint angles [9], [10]. Because humans match their impedance with the environment they are interacting with, which likely varies greatly within a task, system identification methods that can adequately capture this time varying impedance behavior could provide a powerful avenue for investigation.

Initial investigations assumed that impedance parameters remained time invariant during specific tasks. Dyck and Tavakoli [11] proposed a method for computing the impedance of the human arm with time-invariant impedance parameters. They suggested that during controlled motion, the damping coefficient of the human arm is negligible. Along these ideas, it's been shown that for a short time window, joint impedance has varies within a short range [12]. Similar linear time-invariant models for second-order systems were used in Hasser and Cutkosky's study of the human hand [13]. However, in their study with Anklebot, Lee et al. demonstrated the use of time-varying and nonlinear system identification techniques [14], [15]. Eesbeek et al. proposed an identification of time-variant impedance model for wrist joint [16]. Tsumugiwa et al. estimated endpoint limb stiffness using variable impedance control [17]. The estimation of stiffness was carried out using the force and position of the endpoint. They showed that variable impedance behavior provides a benefit from a stability perspective when compared with fixed impedances, further motivating timevarying impedances. More recently, in a simulated study, Cavallo et al. developed a linear second-order impedance identification model, using locally periodic kernels, for timevarying ankle impedance [18].

In this work, we propose a model consisting of periodic impedance parameters. The underlying assumption is that the impedance parameters are periodic with the same period as the task and therefore the method is restricted to steady state behavior during clearly defined periodic tasks with the period known *a priori*. The model is parameterized as a linear time-varying second-order mass-spring-damper system, with periodic stiffness and virtual trajectories. First we demonstrate our method on simulated data. Next, we fit our model to human participant data (N=10) during dynamic interactions with a haptic manipulandum (Fig. 1). The participants were asked to track a periodic trajectory using forearm rotations while the haptic manipulandum behaved with different environmental impedances: i) passive-environment, with no haptic feedback, ii) stiffness-dominant environment,

¹Khandaker Nusaiba Hafiz and Jonathan Realmuto are with the Bionic Systems Lab, Department of Mechanical Engineering, University of California, Riverside. nusaiba.hafiz@email.ucr.edu,jrealmut@ucr.edu

²Terence Sanger is with the Department of Electrical Engineering and Computer Science, University of California, Irvine, and the Children's Hospital of Organe County. tsanger@uci.edu

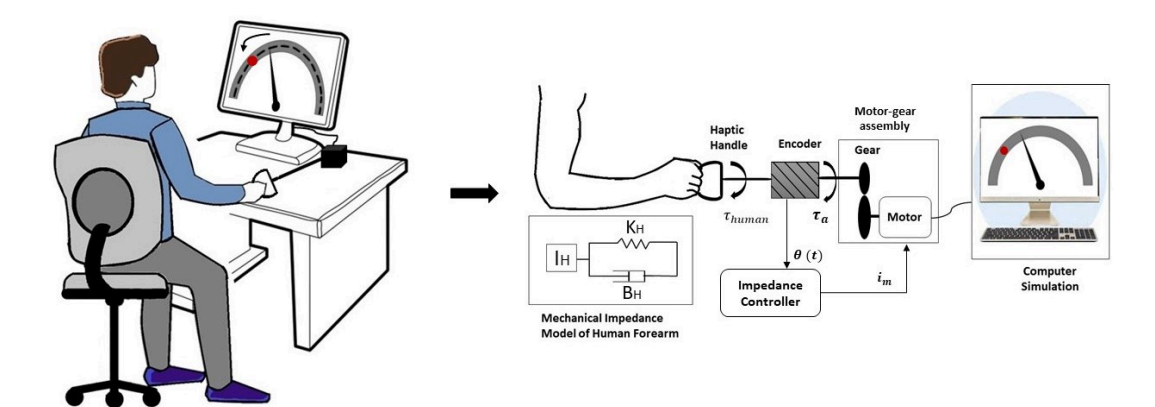


Fig. 1: Schematic representation of experimental setup (left) and details of the impedance modeling (right). The experiment consisted of the human user interacting with a rotational haptic manipulandum. The task was to track a desired periodic trajectory using a cursor controlled by the haptic manipulandum and visualized on the computer screen. The mechanical impedance of the human forearm joint are represented with the parameters I_H , B_H , and K_H . The haptic manipulandum was controlled via an impedance controller with the virtual impedances determining the physical behavior of the manipulandum.

with spring-like behavior, iii) inertia-dominant environment, with virtual inertia, and iv) pendulum environment, dynamics resembling an inverted pendulum.

II. PERIODIC IMPEDANCE MODEL

A. Model Overview

The human impedance model takes the following form:

$$\tau_H(t) = I_H \ddot{\theta}(t) + B_H \dot{\theta}(t) + K_H(t)(\theta(t) - \theta_v(t)) + n(t) \quad (1)$$

$$K_H(t) = K_H(t+T)$$

$$\theta_v(t) = \theta_v(t+T),$$

where $\tau_H(t)$ is the human joint torque, and $K_H(t)$ and $\theta_v(t)$ are the spring coefficient and virtual trajectory of the human forearm, respectively, taken to be periodic with period T, and n(t) is additive zero-mean Gaussian noise. Note that in this work we assume the period T is known a priori and matches the task frequency. The human moment of inertia I_H and damping coefficient B_H are considered scalar parameters. The periodic stiffness term is parameterized as a sum of sines shifted to exclude the possibility of negative stiffness:

$$K_H(t) = \sum_{n=0}^{n} K_n (1 + \sin(n\omega t + \phi_n))$$
 (2)

where K_n and ϕ_n are the amplitude and phase of each harmonic, respectively, and $\omega = \frac{2\pi}{T}$ is the task frequency. Similarly, we parameterize the virtual trajectory as:

$$\theta_{\nu}(t) = \sum_{n=0}^{n} \theta_n \sin(n\omega t + \psi_n)$$
 (3)

where θ_n and ψ_n are the amplitude and phase of each harmonic, respectively.

B. System Identification

The model parameters outlined in (1)-(3) can described using the parameter vector:

$$\mathbf{x} = \begin{bmatrix} I_H & B_H & K_0 & \cdots & K_n & \phi_1 & \cdots & \phi_n & \theta_0 & \cdots & \theta_n & \psi_1 & \cdots & \psi_n \end{bmatrix}.$$

In this work, we choose n=5 harmonics to fit the underlying data. For the system identification procedure, the true torque signal $\tau_H(t)$ and the true angular position $\theta(t)$ are collected, and subsequently the derivatives of $\theta(t)$ are estimated. These four signals provide the data set for the system identification. To find the optimal parameter vector \mathbf{x} , we used the global optimizer toolbox in MATLAB to solve:

$$\min_{\mathbf{x}} \|\tau_H(t) - \hat{\tau}_H(t, \mathbf{x})\|_2$$
subject to: $\underline{\mathbf{x}} \le \mathbf{x} \le \bar{\mathbf{x}}$ (4)

where $\hat{\tau}_H$ is the estimated torque signal, \underline{x} and \bar{x} are the lower and upper bounds of the parameter vector. We used patternsearch and fmincon within a loop to obtain estimates for the parameter vector.

III. SIMULATION STUDY

To verify our methodology we simulated (1) with varying amplitudes of noise n(t). Special care was taken to choose the reference parameter vector such that the resulting system exhibited stable dynamics. We limited the harmonics to n = 5and chose the spectrum of K_H and θ_v to be decreasing with increasing frequency. We used ode45 with a time step of 1/1000 seconds and simulated the system for 15 seconds and a task period of 5 seconds. Using the simulated kinematics and kinetics we used the system identification procedure outlined previously to recover the parameter vector. We repeated the simulated experiment for seven different signalto-noise (SNR) ratios, from 10 to 40 db in increments of 5 dB. The simulated (ground truth) and estimated torque $\tau_H(t)$, stiffness $K_H(t)$, and virtual trajectory $\theta_v(t)$ for SNR of 40, 25, and 10 dB are shown in Fig. 2. We calculated the error for the two time varying parameters (K_H and θ_v) as:

error =
$$\sqrt{\frac{\sum_{t} (p_{\text{true}}(t) - p(t))^{2}}{\sum_{t} (p_{\text{true}}(t))^{2}}}$$
 (5)

where the sums are taken over the time steps. For the two scalar parameters (I_H and B_H), the error was calculated

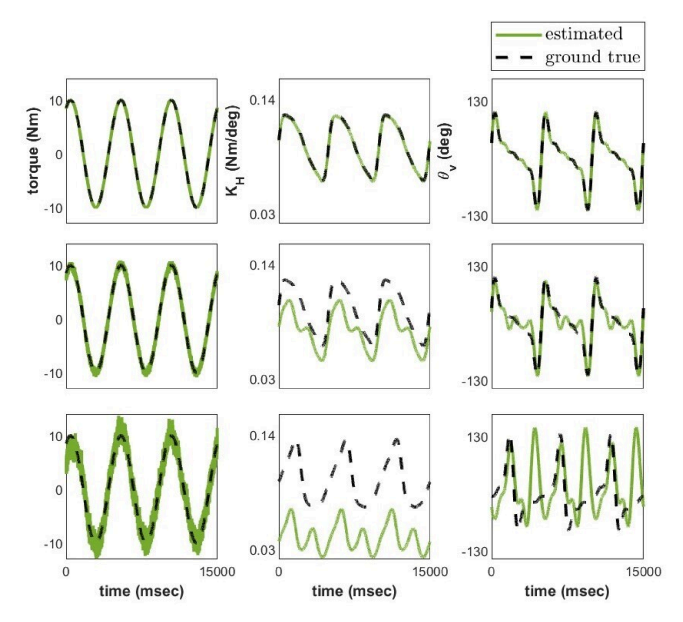


Fig. 2: Simulated (ground truth) and estimated torque $\tau_H(t)$ (left column), stiffness $K_H(t)$ (center column), and virtual trajectory $\theta_v(t)$ (right column) with SNR of 40 (top row), 25 (center row), and 10 (bottom row) dB.

similarly, except the sums in (5) were omitted (since they are scalars). Bar plots for the parameter estimation error for each SNR level are shown in Fig. 3.

IV. EXPERIMENTAL METHOD

A. Setup

The equation of motion for our experiment, as shown in Fig. 1, can be derived as

$$I_e \ddot{\theta}(t) = \tau_a(t) + \tau_H(t) \tag{6}$$

where I_e is the inertia of the shaft (including the handle), which can be calculated from the motor and gearbox's combined moment of inertia, $\tau_a(t)$ is active torque from the motor, and $\tau_H(t)$ is the torque from the human participant. We considered the rotational damping of the handle to be negligible. The external inertia I_e is estimated as

$$I_e = I_{motor}R^2 + I_{gear}$$

where I_{motor} is motor's inertia, $(I_{motor} = 92.5 \text{ gcm}^2)$, I_{gear} is gear's inertia $(I_{gear} = 5 \text{ gcm}^2)$, and R is the gear ratio (R = 36). The external inertia, I_e , for our system was calculated as $0.0119 \text{ Kgm}^2/\text{degree}$.

B. Participants

Ten participants (9 men and 1 woman) with no known neuro-muscular disabilities ranging in age from 20 to 33 years old (mean age = 22.4, standard deviation = 4.27) were recruited to participant in this study. The study was reviewed and approved by the University of Southern California Institutional Review Board¹ and written informed consent to participate was provided by each participant.

¹Authors Realmuto and Sanger were previously affiliated with the University of Southern California were the study was conducted.

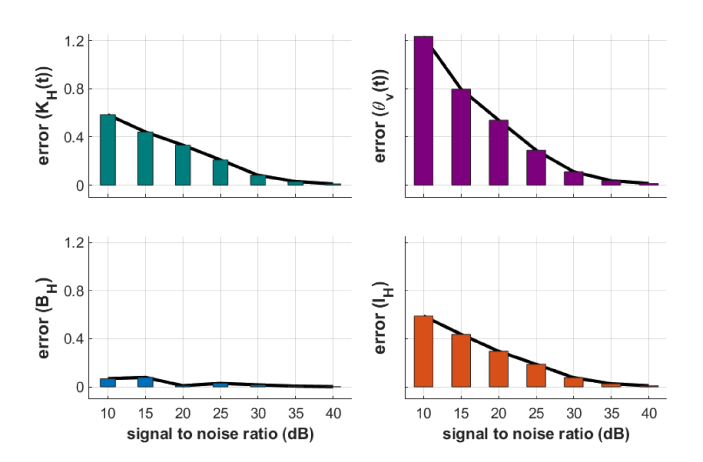


Fig. 3: Parameter errors for all SNR trials demonstrating our method is relatively accurate with SNR under 25 dB.

C. Virtual Environments and Haptic Manipulandum

Figure 1 shows the experimental setup used in this study, which involved the participant holding the handle of a rotational haptic manipulandum with one degree-of-freedom. The haptic manipulandum comprised of a brushless DC motor and gearhead (EC 45 Flat, 42.9 mm, 30W brushless motor, and 36:1 Planetary Gearhead, Maxon, Switzerland) attached to a shaft with a handle for the participant to interact with. Angular feedback was provided by an encoder at the shaft (AMT20 Series, CUI Devices, USA). The motor was directly controlled by a Beaglebone Black development platform, operating at a loop frequency of 1 kHz, through an external motor current control board (ESCON 36/3 EC, 4-Q Servocontroller for EC motors, Maxon, Switzerland) that took an analog set point for the desired motor current as input. The motor, gear, encoder, and haptic manipulandum were securely assembled onto a table in a fixed position. A computer screen next to the device displayed the desired tracking trajectory on a semi-circular display and the participants were asked to follow that trajectory. The participants' current position also appeared on the display. To generate interaction torques and simulate dynamic environments, an impedance controller was employed [19]. The active torque of the haptic manipulandum was proportional to the motor current:

$$\tau_a(t) = -Rk_{\tau}i_m(t)$$

where R (= 36) was the gear ratio, k_{τ} (= 0.0255 Nm/A) the torque constant, and i_m the motor current. The motor current was modulated for each environment as follows:

$$i_{m}(t) = \begin{cases} 0 & \text{Passive} \\ K_{\nu}\theta(t) & \text{Spring} \\ I_{\nu}\ddot{\theta}_{f}(t) & \text{Inertia} \\ I_{\nu}(\ddot{\theta}_{f}(t) + g(\sin(\theta(t))) & \text{Pendulum} \end{cases}$$
(7)

where K_{ν} and I_{ν} are the virtual impedance parameters, $\theta(t)$ the feedback signal for the angular position, $\ddot{\theta}_f(t)$ the real-time estimate of the angular acceleration, and g the gravitational constant, take as g=1 in this study.

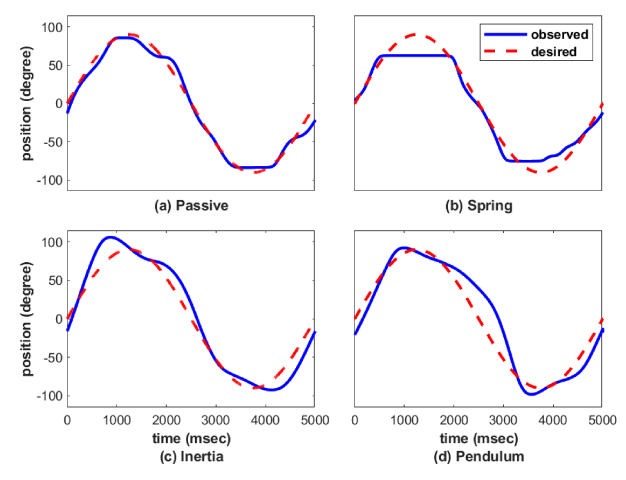


Fig. 4: Observed (blue) and desired (red) angular position of one participant during one cycle for all four environments.

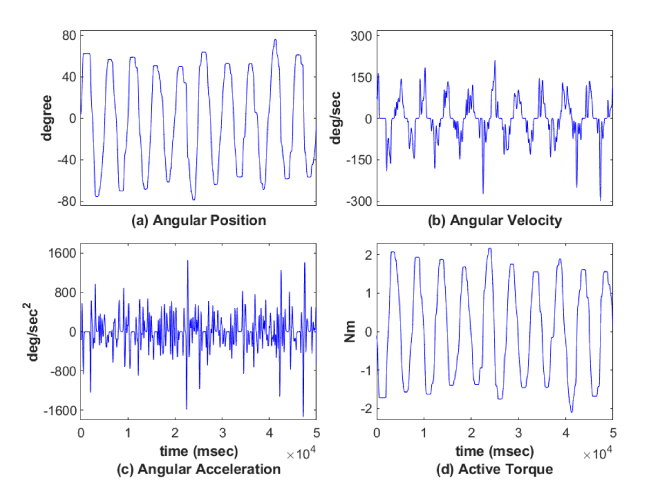


Fig. 5: Angular position, angular velocity, angular acceleration, and active torque for one trial in the spring environment.

D. Experimental Procedure

Each participant experienced four distinct dynamic environments, as outlined in (7): Passive, Stiffness, Inertia, and Pendulum environments, which were achieved via the haptic manipulandum impedance controller as shown in Fig. 1. In the Passive environment, the virtual impedance parameters were set to zero, so the system did not incorporate any additional torque from the impedance controller. In the other three environments (Spring, Inertia, and Pendulum) the impedance controller was active and provided torque to the system based on the virtual impedance parameters, e.g., the spring coefficient and moment of inertia as shown in (7). This means that the system's response was determined by the impedance controller. Specifically, the Spring environment emphasized the effect of the spring coefficient, while the Inertia environment emphasized the effect of the moment of inertia, and the Pendulum environment was designed to simulate an inverted pendulum. In the Spring environment, the virtual impedance parameters were chosen as $K_{\nu} = 0.03$ Nm/degree and $I_v = 0$. In the Inertia environment, the virtual impedance parameters were chosen as $I_v = 5 \text{ Nms}^2$ and

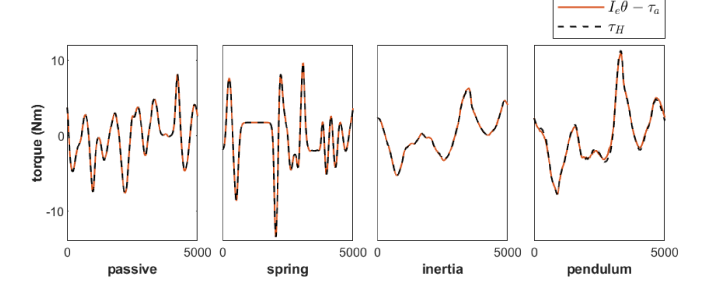


Fig. 6: Fitted torques signals over a single cycle from the system identification model parameters for four environments.

 $K_v = 0$. In the Pendulum environment, g = 1 and $I_v = 5$ Nms². These experimental parameters were carefully chosen to avoid instability during human interactions through an iterative tuning process completed prior to the experiments. The experiment was divided into five blocks, where in each block the participant completed four trials, one for each environment. During each trial, the participant was required to follow a sinusoidal trajectory of 15 cycles at 0.2 Hz, ranging from -80° to 80°. In the first block the environments appeared in the following order: Passive, Stiffness, Inertia, Pendulum. In all subsequent blocks the order of the environments was randomized. To minimize the effect of learning and transient adaptation, we included only the last ten cycles of the last experimental block for analysis. Figure 4 shows representative trials of the observed and desired angular position for one participant during all four dynamics environments over a single cycle.

E. System Identification Details

Our model is outlined in (1)-(3). We chose n=5 harmonics to fit the model to the human participant data. For the system identification procedure, the reference torque signal is take as $\tau_H = I_e \ddot{\theta}(t) - \tau_a(t)$, and therefore the active torque τ_a and the angular position $\theta(t)$ were collected, and subsequently the derivatives of $\theta(t)$ are estimated. These four signals provide the data set for the system identification and a representing trial is shown in Fig. 5. We use the same optimization problem in (4).

V. RESULT

We estimated the parameters of the periodic impedance model using system identification for all N=10 participants in all four dynamics environments. Using these parameters, we estimated the human torque signal using (1), and as shown in Fig. 6, the human torque values provide an excellent fit to the underlying data. The average estimated parameters for the damping coefficient (B_H) and moment of inertia (I_H) during the four distinct dynamic environments are shown in Table I. The periodic impedance parameters for all subjects across all environments are shown in Fig. 7.

VI. DISCUSSION

Here, we introduced a periodic impedance model, showed through simulation it produces valid estimations at various

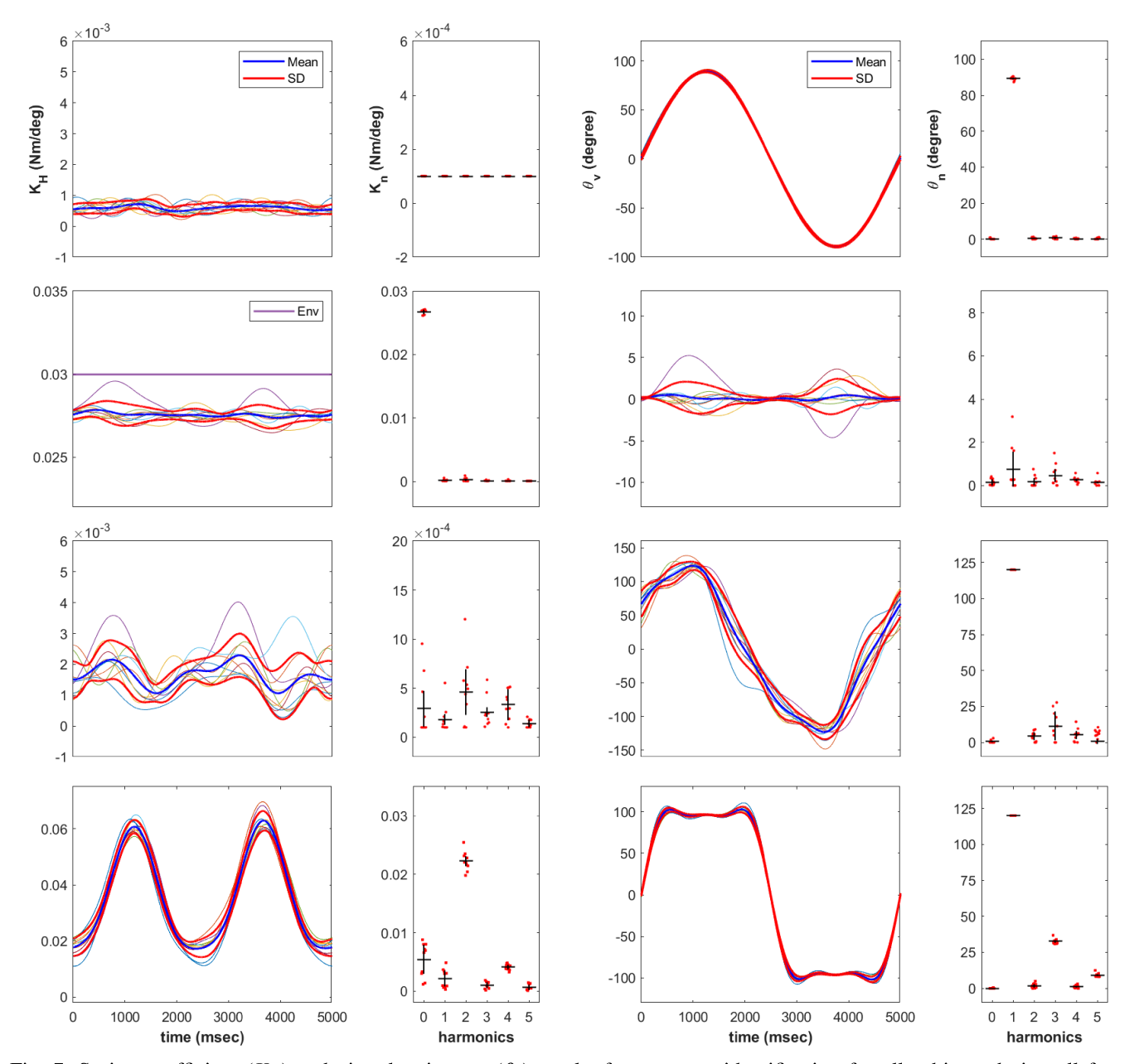


Fig. 7: Spring coefficient (K_H) and virtual trajectory (θ_v) results from system identification for all subjects during all four environments. From left to right: K_H in the time domain, K_n in the frequency domain, θ_v in the time domain, θ_n in the frequency domain. First row: Passive Environment. Second row: Spring Environment. Third row: Inertia Environment. Last row: Pendulum Environment. On time domain plots red traces represent \pm one-standard deviation, blue traces are the population average, and other colors are the individual participants. On frequency domain plots, red dots represent the individual participants' parameters, vertical black line represents the interquartile range, and horizontal black line the population average.

noise levels, and fit the model to N=10 participants across four different environments using system identification. The average R-squared, calculated using the true human torque signal and the estimated human torque signal, over all environments and participants was found to be around $R^2 = 0.99$. The high average R-squared value indicates the model is capable of accurately capturing the dynamic interactions, however further analysis is required to elucidate whether the model is over-fitting.

Of note is the variability in estimated parameters across the four dynamic environments and the absence of variability across participants within each environment. For the first two environments (Passive and Spring), the identified stiffness coefficient was not periodic, but nearly constant. More interesting is that the stiffness coefficient during the Spring environment is close to the environmental virtual stiffness ($K_{\nu} = 0.03$), as can be seen in the first and second columns, second row in Fig. 7. This suggests that participants

were impedance matching with the environment, perhaps to maximize mechanical power transfer, and supports the idea that humans adapt their impedance to the task.

During the Pendulum environment, our analysis suggests that time-varying stiffness is important, evident from the consistent spring coefficient traces across participants in the last row of Fig. 7. We also note the consistent virtual trajectory across subjects, suggesting a consistent motor control strategy across participants.

While the general approach to impedance system identification leverages external perturbations to evoke responses, we explored fitting parameterized periodic models directly to periodic task data. The major assumption is that during steady state cyclic behavior, when learning and transients do not dominate the response, the time varying impedances are periodic with the same task frequency. While this assumption is not necessary for dynamic stability, it greatly simplifies the identification problem and a limitation of our method.

Care is required for implementation and interpretation of our method. The solution is sensitive to the choice in the upper and lower bounds, and further investigation is required to understand the uniqueness of the solution, as it is be possible to arrive at multiple (locally optimal) parameter vectors that result in the same trajectories. Over-fitting is also possible. While we are confident our technique can capture the general trend, it does not fully encapsulate the intricacies of muscle activation and joint mechanics. This is evident in our results which have inertia variations on the order 30% between the Passive and Pendulum environments. The variation in inertia is probably due to unmodeled dynamics that are accounted for in model's inertia term. Future work will aim at minimizing these limitations through more comprehensive simulation studies, controlled human experiments, and a comprehensive comparison between impedances models.

VII. CONCLUSION

The process of system identification in human movement serves as a valuable tool for gaining deeper insights into the underlying mechanisms of motor control and coordination. The development and successful testing of the periodic impedance model represent a step forward in understanding human-robot interactions. The simulation study and high average R-squared values for all environment indicates the reliability of our model. The sensitivity we observed to changing environments emphasizes the importance of employing adaptable control strategies in different situations. The phenomenon of impedance matching further emphasizes

TABLE I: Damping co-efficient (B_H) and moment of inertia (I_H) for all environments.

Environments	Damping Co-efficient B_H (Ns/m)	Moment of Inertia $I_H \text{ (Nms}^2\text{)}$
Passive	3.30×10^{-6}	0.0144
Spring-Dominant	9.66×10^{-6}	0.0144
Inertia-Dominant	0	0.0198
Pendulum	4.53×10^{-4}	0.0207

the adaptability and sophistication of human motor control mechanisms. The findings from this research have implications for various domains, including as a crucial tool in the development of advanced prosthetic devices, enhancing rehabilitation robotics, and enabling more natural interactions in collaborative settings.

REFERENCES

- [1] D. W. Franklin and D. M. Wolpert, "Computational mechanisms of sensorimotor control," *Neuron*, vol. 72, no. 3, pp. 425–442, 2011.
- [2] N. Hogan, "Adaptive control of mechanical impedance by coactivation of antagonist muscles," *IEEE Transactions on automatic control*, vol. 29, no. 8, pp. 681–690, 1984.
- [3] —, "The mechanics of multi-joint posture and movement control," Biological cybernetics, vol. 52, no. 5, pp. 315–331, 1985.
- [4] E. Burdet, R. Osu, D. W. Franklin, T. E. Milner, and M. Kawato, "The central nervous system stabilizes unstable dynamics by learning optimal impedance," *Nature*, vol. 414, no. 6862, pp. 446–449, 2001.
- [5] R. Osu and H. Gomi, "Multijoint muscle regulation mechanisms examined by measured human arm stiffness and emg signals," *Journal* of neurophysiology, vol. 81, no. 4, pp. 1458–1468, 1999.
- [6] E. J. Perreault, R. F. Kirsch, and P. E. Crago, "Multijoint dynamics and postural stability of the human arm," *Experimental brain research*, vol. 157, no. 4, pp. 507–517, 2004.
- [7] P. K. Artemiadis, P. T. Katsiaris, M. V. Liarokapis, and K. J. Kyriakopoulos, "Human arm impedance: Characterization and modeling in 3d space," in 2010 IEEE/RSJ International Conference on Intelligent Robots and Systems. IEEE, 2010, pp. 3103–3108.
- [8] H. Gomi and R. Osu, "Task-dependent viscoelasticity of human multijoint arm and its spatial characteristics for interaction with environments," *Journal of neuroscience*, vol. 18, no. 21, pp. 8965– 8978, 1998.
- [9] D. W. Franklin, G. Liaw, T. E. Milner, R. Osu, E. Burdet, and M. Kawato, "Endpoint stiffness of the arm is directionally tuned to instability in the environment," *Journal of Neuroscience*, vol. 27, no. 29, pp. 7705–7716, 2007.
- [10] R. D. Trumbower, M. A. Krutky, B.-S. Yang, and E. J. Perreault, "Use of self-selected postures to regulate multi-joint stiffness during unconstrained tasks," *PloS one*, vol. 4, no. 5, p. e5411, 2009.
- [11] M. Dyck and M. Tavakoli, "Measuring the dynamic impedance of the human arm without a force sensor," in 2013 IEEE 13th International Conference on Rehabilitation Robotics (ICORR). IEEE, 2013, pp. 1–8
- [12] D. Ludvig and E. J. Perreault, "System identification of physiological systems using short data segments," *IEEE Transactions on Biomedical Engineering*, vol. 59, no. 12, pp. 3541–3549, 2012.
- [13] C. J. Hasser and M. R. Cutkosky, "System identification of the human hand grasping a haptic knob." in Symposium on haptic interfaces for virtual environment and teleoperator systems. Orlando, FL, USA, 2002, p. 180.
- [14] H. Lee and N. Hogan, "Time-varying ankle mechanical impedance during human locomotion," *IEEE Transactions on Neural Systems and Rehabilitation Engineering*, vol. 23, no. 5, pp. 755–764, 2014.
- [15] H. Lee, H. I. Krebs, and N. Hogan, "Multivariable dynamic ankle mechanical impedance with active muscles," *IEEE Transactions on Neural Systems and Rehabilitation Engineering*, vol. 22, no. 5, pp. 971–981, 2014.
- [16] S. van Eesbeek, F. van der Helm, M. Verhaegen, and E. de Vlugt, "Lpv subspace identification of time-variant joint impedance," in 2013 6th International IEEE/EMBS Conference on Neural Engineering (NER). IEEE, 2013, pp. 343–346.
- [17] T. Tsumugiwa, R. Yokogawa, and K. Hara, "Variable impedance control based on estimation of human arm stiffness for human-robot cooperative calligraphic task," in *Proceedings 2002 IEEE International Conference on Robotics and Automation (Cat. No. 02CH37292)*, vol. 1. IEEE, 2002, pp. 644–650.
- [18] G. Cavallo, A. C. Schouten, and J. Lataire, "Locally periodic kernel-based regression to identify time-varying ankle impedance during locomotion: A simulation study," in 2020 42nd Annual International Conference of the IEEE Engineering in Medicine & Biology Society (EMBC). IEEE, 2020, pp. 4835–4838.
- [19] N. Hogan and S. P. Buerger, "Impedance and interaction control," in Robotics and automation handbook. CRC press, 2018, pp. 375–398.